

**The following resources related to this article are available online at
www.sciencemag.org (this information is current as of October 8, 2009):**

Updated information and services, including high-resolution figures, can be found in the online version of this article at:
<http://www.sciencemag.org/cgi/content/full/326/5950/248>

Supporting Online Material can be found at:
<http://www.sciencemag.org/cgi/content/full/326/5950/248/DC1>

This article **cites 60 articles**, 11 of which can be accessed for free:
<http://www.sciencemag.org/cgi/content/full/326/5950/248#otherarticles>

This article has been **cited by** 1 articles hosted by HighWire Press; see:
<http://www.sciencemag.org/cgi/content/full/326/5950/248#otherarticles>

This article appears in the following **subject collections**:
Atmospheric Science
<http://www.sciencemag.org/cgi/collection/atmos>

Information about obtaining **reprints** of this article or about obtaining **permission to reproduce this article** in whole or in part can be found at:
<http://www.sciencemag.org/about/permissions.dtl>

Ice Age Terminations

Hai Cheng,¹ R. Lawrence Edwards,^{1*} Wallace S. Broecker,² George H. Denton,³ Xinggong Kong,⁴ Yongjin Wang,⁴ Rong Zhang,⁵ Xianfeng Wang¹

²³⁰Th-dated oxygen isotope records of stalagmites from Sanbao Cave, China, characterize Asian Monsoon (AM) precipitation through the ends of the third- and fourthmost recent ice ages. As a result, AM records for the past four glacial terminations can now be precisely correlated with those from ice cores and marine sediments, establishing the timing and sequence of major events. In all four cases, observations are consistent with a classic Northern Hemisphere summer insolation intensity trigger for an initial retreat of northern ice sheets. Meltwater and icebergs entering the North Atlantic alter oceanic and atmospheric circulation and associated fluxes of heat and carbon, causing increases in atmospheric CO₂ and Antarctic temperatures that drive the termination in the Southern Hemisphere. Increasing CO₂ and summer insolation drive recession of northern ice sheets, with probable positive feedbacks between sea level and CO₂.

The “sawtooth” character of late Quaternary ice-age cycles, with gradual buildup and rapid collapse of ice sheets, has been known since Emiliani’s pioneering oxygen isotope ($\delta^{18}\text{O}$) measurements on marine sediments (1). Explanations of the rapid collapses, dubbed “terminations” (2), have long been sought. The ice-age cycles have been linked to changes in Earth’s orbital geometry (the Milankovitch or Astronomical theory) through spectral analysis of marine oxygen-isotope records (3), which demonstrate power in the ice-age record at the same three spectral periods as orbitally driven changes in insolation. However, explaining the 100 thousand-year (ky)-recurrence period of ice ages has proved to be problematic because although the 100-ky cycle dominates the ice-volume power spectrum, it is small in the insolation spectrum. In order to understand what factors control ice age cycles, we must know the extent to which terminations are systematically linked to insolation and how any such linkage can produce a non-linear response by the climate system at the end of ice ages.

Answering such questions depends on establishing the precise timing of a number of terminations relative to changes in insolation. Recent improvements in the precision and accuracy of ²³⁰Th dating techniques have substantially increased our ability to determine absolute ages for CaCO₃ (4) and thus allow us to establish the exact timing of climate events preserved in some types of cave deposits. For the last glacial period,

it has been shown that times of unusually high $\delta^{18}\text{O}$ in speleothems from Chinese caves correlate with Heinrich events (5) recorded in North Atlantic marine sediments (6, 7). Because portions of each of the last four terminations coincide with a major Heinrich event (8), we can establish the timing of marine oxygen-isotope terminations by correlating North Atlantic ice rafted debris (IRD) to radiometrically dated oxygen-isotope cave records from China (6).

Variations in atmospheric methane concentration, as revealed in ice cores, correlate with changes in $\delta^{18}\text{O}$ in speleothems from Chinese caves (6, 7) for the major climate events of the last glacial period. The last two terminations also were accompanied by abrupt $\delta^{18}\text{O}$ shifts that correlate with sharp methane changes (6, 7). Here, we show that the two next-oldest terminations [Termination III (T-III) and IV (T-IV)] also have corresponding shifts in methane and cave $\delta^{18}\text{O}$. Thus, we are able to determine the timing of events recorded in Antarctic ice cores by correlating them to the radiometrically dated cave record (6, 9). Using the cave-marine and cave-ice-core correlations, we ascertained for each of the last four terminations the timings of the ma-

rine termination, the CO₂ rise, the Antarctic temperature rise, the shift in the $\delta^{18}\text{O}$ of atmospheric O₂, and the lowering of dust flux to Antarctica. We then compared the timing of these changes to the known variations in insolation.

We have previously reported AM data for T-I (7, 10) and T-II (6, 9). Here, we confirm the T-II data at yet higher resolution (Fig. 1) and present data for T-III and T-IV. In all cases, we correlate the monsoon signature both to marine and to ice-core records. By comparing and contrasting the character and sequence of events in all four terminations, we make plausible inferences regarding processes that cause terminations.

The highest-resolution data for T-III and T-IV are from Sanbao Cave, which augment the existing record (11). We also present Sanbao data for T-II and for the precession cycle after T-III, which includes an interval of time that we call T-IIIa [the shift from Marine Isotope Stage (MIS) 7.4 to 7.3]. Finally, we report data from two stalagmites from nearby Linzhu Cave, which corroborate the Sanbao data.

Chinese caves and the oxygen-isotopic composition of cave calcite.

Sanbao (SB) and Linzhu (LZ) caves are located in Hubei province, central China, on the northern slope of Mountain Shennongjia, near the southern edge of the Chinese Loess Plateau (110°26'E, 31°40'N, elevation 1900 m and 110°19'E, 31°31'N, elevation 780 m, respectively) (fig. S1). The area is currently affected by the summer AM, with a mean annual precipitation of 1900 to 2000 mm and mean annual temperature between 8 and 9°C. During summer (June through September), the inland flow of warm/humid air from the tropical Indo-Pacific penetrates to the northern slope of Mountain Shennongjia, delivering about 80% of the total annual precipitation.

We obtained precise ages (± 100 years for T-II, ± 800 years for T-III, and ± 1500 years for T-IV) using a recently developed ²³⁰Th dating technique (fig. S2 and table S1) (4). Subsamples for oxygen-isotope measurements (table S2) had temporal spacings of 20 to 70 years.

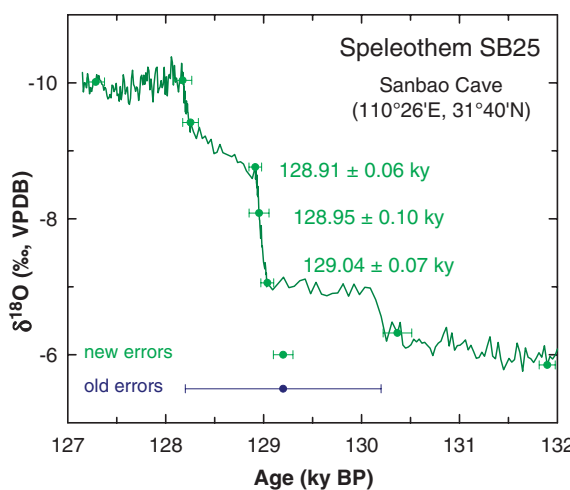


Fig. 1. The $\delta^{18}\text{O}$ time series showing the abrupt shift in the AM during T-II, as recorded in Sanbao Cave. This feature was previously observed in Dongge Cave (9) and Hulu Cave (6), as well as Sanbao Cave (11); however, the new dating methods applied here constrain the age of this feature to lie within a century of 129.0 ky B.P. This date agrees with previous dates; however, the errors reported here are about an order of magnitude smaller than those reported in the earlier studies.

¹Department of Geology and Geophysics, University of Minnesota, Minneapolis, MN 55455, USA. ²Lamont-Doherty Earth Observatory of Columbia University, 61 Route 9W, Post Office Box 1000, Palisades, NY 10964–1000, USA. ³Department of Earth Sciences, Bryand Global Sciences Center, Climate Change Institute, University of Maine, Orono, ME 04469, USA. ⁴College of Geography Science, Nanjing Normal University, Nanjing 210097, China. ⁵National Oceanic and Atmospheric Administration (NOAA)/Geophysical Fluid Dynamics Laboratory, Princeton, NJ 08540, USA.

*To whom correspondence should be addressed. E-mail: edwar001@umn.edu

On the basis of the replication test (Figs. 2, 3, and 4 and fig. S3) (12) and other lines of reasoning (4), most of the variability in our records results from changes in the $\delta^{18}\text{O}$ of precipitation. We interpret these changes following the original reasoning of Wang *et al.* [(7); see also (6, 9)], who noted that (i) most precipitation in southeastern China is summer monsoon rainfall, with distinctly lower $\delta^{18}\text{O}$ than precipitation during the rest of the year, and (ii) the effect of mean summer temperature or precipitation on mean summer $\delta^{18}\text{O}$ is small, as is the case for winter. Thus, neither the temperature- $\delta^{18}\text{O}$ relationship, commonly used to interpret ice-core data, nor the interpretation based on the “amount effect” (13) is justified, as confirmed by Johnson and Ingram (14). Instead, Wang *et al.* (7) suggested that a changing ratio of low- $\delta^{18}\text{O}$ (summer monsoon) rainfall to high- $\delta^{18}\text{O}$ (rest of the year) rainfall could explain the cave isotopic data. Because the low- $\delta^{18}\text{O}$ rainfall has a distant tropical Indo-Pacific source (6) and the high- $\delta^{18}\text{O}$ precipitation probably has a more local oceanic source, the Wang *et al.* interpretation invokes varying proportions of rainfall from these two sources to explain the data. To the extent that the ratio of low- to high- $\delta^{18}\text{O}$ precipitation correlates with the absolute amount of low- $\delta^{18}\text{O}$ (summer monsoon) precipitation, we can view the cave record as a measure of the amount of summer monsoon precipitation or “summer monsoon intensity.” Because cave records from sites across southern

Asia have similar signatures (6, 9, 11, 15–17), the $\delta^{18}\text{O}$ variations probably result from broad changes in atmospheric circulation, which shift moisture sources and rainfall patterns across the whole southern Asia region. A simple example would be a change in the fraction of the year dominated by the summer monsoon circulation pattern. Such a process could easily account for the large observed range in cave $\delta^{18}\text{O}$, in view of the fact that the modern seasonal range is even larger.

Correlations with North Atlantic climate.

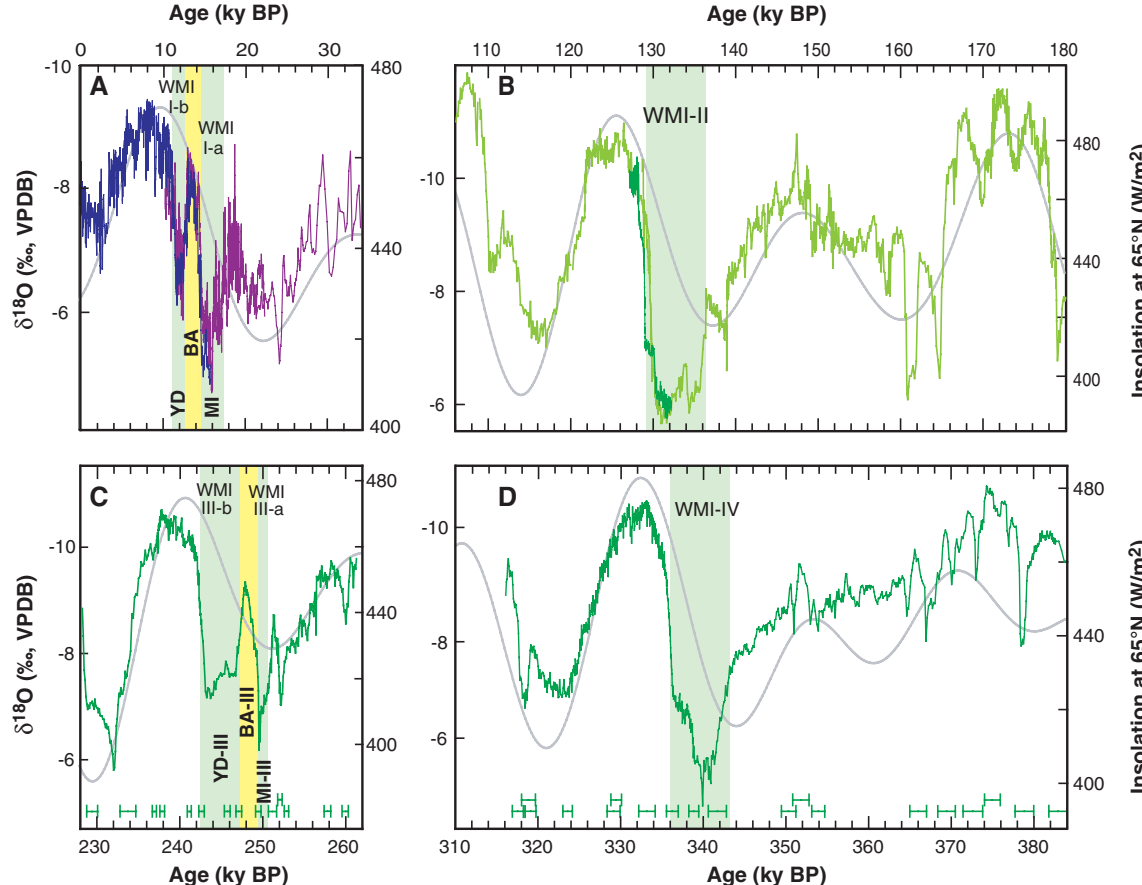
Chinese cave $\delta^{18}\text{O}$ records (6, 7, 9–11, 17) have clear correlations with (i) summer insolation (Fig. 4) and (ii) North Atlantic climate. The most striking of these links (7) are the close correspondence between the monsoon and the Greenland stadial-interstadial sequences (18) and the tie between high cave $\delta^{18}\text{O}$ and Heinrich events (19). The link to Heinrich events suggests that the monsoon responds to the breakup of the Laurentide Ice Sheet. This is supported by T-I and T-II cave records (Fig. 2), for which the monsoon generally follows summer insolation, with the distinct exception of “gouges” (times of weak monsoon) that correlate broadly to Heinrich stadial I (H-I) and to the Younger Dryas (during T-I) and to H-11 (during T-II). We interpret these gouges as times when the monsoon deviated from a simple insolation response because of cold anomalies generated by ice-sheet disintegration and the resulting influx of meltwater and icebergs

to the North Atlantic. The influx could trigger an anomaly by reducing meridional overturning circulation (MOC) and associated northward surface-ocean transport of heat (20, 21).

Sea-ice formation would amplify the anomaly (22), particularly during winter, causing pronounced seasonality in the North Atlantic region (23, 24). Extensive winter sea ice cover would seal off the escape of heat to the atmosphere, causing winter temperatures to plunge, generating a climate akin to that of Siberia today. This winter anomaly would probably advect eastward into the northern Indian Ocean and Eurasia, affecting the summer monsoon (25, 26), as observed in the Chinese cave records. Alternately, the monsoon may respond through shifts in both Hadley and Walker circulation triggered by the anomaly (27). The sea-ice mechanism and associated seasonality may help to explain an apparent paradox in our scenario. How can the northern ice sheets retreat at times when the North Atlantic is cold? The answer may be that the cold anomaly is largely a winter phenomenon. The glaciers would melt during the relatively warm summers but would not be strongly affected by the unusually cold winters (23).

Denton *et al.* (28) provided an overview of the main events (including the early stages of the termination itself) that took place at about the time of H-1 [17.5 to 14.5 ky before the present (B.P.)] and termed it the “Mystery Interval” (MI). Cheng *et al.* (6) subsequently identified an

Fig. 2. The $\delta^{18}\text{O}$ time series over the past four glacial terminations from (A) Hulu and Dongte caves (7, 10), (B) Sanbao Cave [light green (11) and dark green SB25 (this study)], and (C and D) Sanbao Cave [sample SB61 (this study)]. Error bars indicate ^{230}Th dates and 2σ errors. $\delta^{18}\text{O}$ increases downward. 21 July insolation at 65°N (29) is in gray. Light green bars depict the WMIs. Similarities between T-I and T-III and between T-II and T-IV are apparent. Analogous to the MI, BA (yellow bar), and YD events during T-I, we identify similar events during T-III: MI-III, BA-III (yellow bar), and YD-III. The light green bars WMI-Ia and WMI-Ib (YD); WMI-II, WMI-IIIa, and WMI-IIb (YD-III); and WMI-IV indicate WMIs.



analogous MI during T-II (MI-II, 136 to 129 ky B.P.), which includes most of the termination and corresponds to the H-11 stadial in the North Atlantic. They termed the monsoon during this time the “Weak Monsoon Interval” (WMI-II). T-I and T-II monsoons have similar total lengths of weak monsoons (T-I, 4600 years for the combined duration of MI-I and the YD; T-II, 6000 years). In both cases, the WMI or the pair of WMIs ended with an abrupt shift to low $\delta^{18}\text{O}$, which was maintained for about 10 ky during the subsequent interglacial period. However, the weak monsoon of T-I is interrupted by an interstadial [the Bølling-Allerød (BA)] lasting 1800 years, whereas the weak monsoon of T-II is punctuated

by an interstadial (at 134 ky B.P.) no more than several hundred years in length (Fig. 2).

Our data show that WMIs occurred during T-III and T-IV (Fig. 2), too. The monsoon during T-III has a signature similar to that of T-I, with two WMIs. WMI-IIIa lasted about 2000 years from 251 to 249 ky B.P. WMI-IIIb lasted about 4500 years from 247 to 242.5 ky B.P. Thus, the total duration of T-III WMIs was 6500 years. As in T-I, the WMIs of T-III are separated by a long interstadial that lasted ~2000 years from 249 to 247 ky B.P. By analogy to the BA, we term this long interstadial the Bølling-Allerød-III (BA-III) and the subsequent WMI the Younger Dryas-III (YD-III). The monsoon signature during T-IV

has a simpler structure, with one long WMI (WMI-IV) lasting about 7000 years from 343 to 336 ky B.P. and ending with an abrupt shift as in the other terminations. The monsoon during T-IV is close in structure to that during T-II, although we see no evidence for even a short interstadial punctuating WMI-IV. In sum, the monsoon during each of the last four terminations features one or two WMIs with total lengths of several millennia. The WMI (or WMIs) begins when boreal summer insolation intensity (29) is low but increasing (Fig. 2). The remainder of the WMI (or WMIs) coincides with the rising limb of the boreal insolation curve (Fig. 2). If the WMIs represent the response to North Atlantic cold anomalies from ice-sheet disintegration, these observations suggest that classic Milankovitch boreal summer insolation rise acting on northern ice sheets is one of the drivers of terminations.

Further support for this idea comes from IRD/Heimrich stadial records from North Atlantic sediments (8). The Ocean Drilling Program (ODP) 980 core has maxima in IRD (8) at about the time of each of our WMIs (Fig. 2). Indeed, for T-III, we observe two IRD peaks, which correspond to WMI-IIIa and WMI-IIIb, and even a third smaller IRD peak that corresponds to an earlier weak monsoon episode (at 252 ky B.P.). By correlating the IRD peaks to the dated WMIs, we established the timing of each termination as recorded by benthic $\delta^{18}\text{O}$ values. We observe that (i) the benthic $\delta^{18}\text{O}$ values begin decreasing at the beginning of the first WMI in each termination and (ii) much of each benthic marine termination takes place during the WMIs. These observations substantiate the view that the WMIs represent the response of the monsoon to a North Atlantic cold anomaly caused by disintegrating ice sheets and amplified through sea-ice formation.

Northern Hemisphere summer insolation. As with the WMIs, each marine termination begins when boreal summer insolation intensity is low but rising, with much of the remainder taking place during the rising limb of the insolation curve (Fig. 3). The first observation suggests that the termination is initially triggered by rising insolation, whereas the second observation suggests that rising insolation plays a role in driving the termination to completion. There is a lack of a clear lag between insolation rise and ice-sheet response. Thus, a several-thousand-year lag, commonly assumed in astronomical tuning of marine oxygen-isotope records (30), does not seem to occur during terminations. This apparent sensitivity is a point that is relevant for projecting the future behavior of today’s glaciers (31, 32) in a higher- CO_2 world.

If insolation is the trigger, why do terminations not occur every time that insolation rises from a low value (Fig. 4)? An additional necessary condition could be the presence of a massive, isostatically compensated ice sheet (33–35) whose collapse was triggered by a rise in summer insolation intensity. All other factors being equal, isostatic compensation would lower the ice-sheet

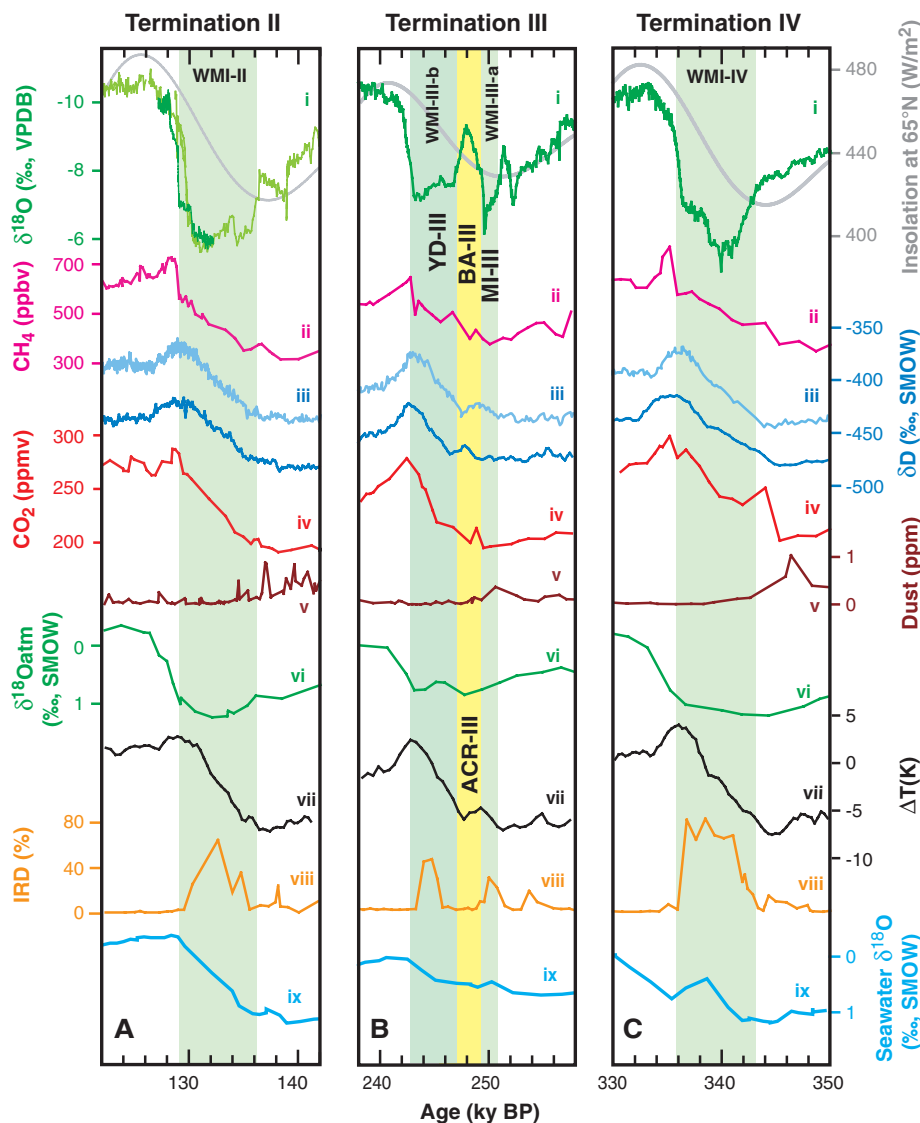


Fig. 3. Events during (A) T-II, (B) T-III, and (C) T-IV. (i) Sanbao $\delta^{18}\text{O}$, colors and sources as in Fig. 2. Light green bars indicate WMIs; yellow bars indicate the YD-III and BA-III/ACR-III. 21 July insolation at 65°N is plotted in gray (29). Antarctic records of (ii) CH_4 (36), (iii) δD [dark blue, Vostok (36), light blue EPICA/Dome C (39)], (iv) CO_2 (36), (v) dust (36), (vi) $\delta^{18}\text{O}$ of O_2 (36), and (vii) Vostok temperature deviation (40). North Atlantic sediment (ODP 980) records (8) of (viii) IRD and (ix) benthic $\delta^{18}\text{O}$ are also shown. All records are plotted on their original time scales but shifted so that the abrupt cave $\delta^{18}\text{O}$ shifts and the marine IRD peaks correlate with the high- $\delta^{18}\text{O}$ cave excursions. The Antarctic records with O_2/N_2 chronologies were shifted no more than 2.2 ky, within quoted errors.

surface, thereby increasing both the average surface temperature and the area of the ice sheet grounded below sea level. Both of these responses would predispose an ice sheet to collapse.

The amount and rate of insolation rise may also be important controls on ice sheets. All four terminations occur when the magnitudes of insolation rise (Fig. 4B), along with the maximum in the rate of insolation rise (Fig. 4C), are average or above average in value, which may be critical in driving the termination to completion. Supporting this idea is the observation that the two terminations (T-I and T-III) interrupted by interstadials (BA and BA-III) are associated with relatively low insolation shifts and rates of insolation change. In contrast, the uninterrupted (T-IV) and minimally interrupted (T-II) terminations are associated with high shifts and rates. Additional observations also support this view. The lowest insolation value in the last 400 ky is at 229 ky B.P., and the highest is at 218 ky B.P., with the highest magnitude and rate of rise occurring between these times (Fig. 4, B and C). The highest $\delta^{18}\text{O}$ values (corresponding to the weakest monsoon) in the Sanbao record is between 227 to 229 ky B.P. (Fig. 4 and fig. S5), corresponding to the beginning of the insolation rise. On the basis of its correlation to an IRD peak in ODP 980 (8), we observe that this event takes place during the early portion of the transition from MIS 7.4 to MIS 7.3. Moreover (as described below for the main terminations), by

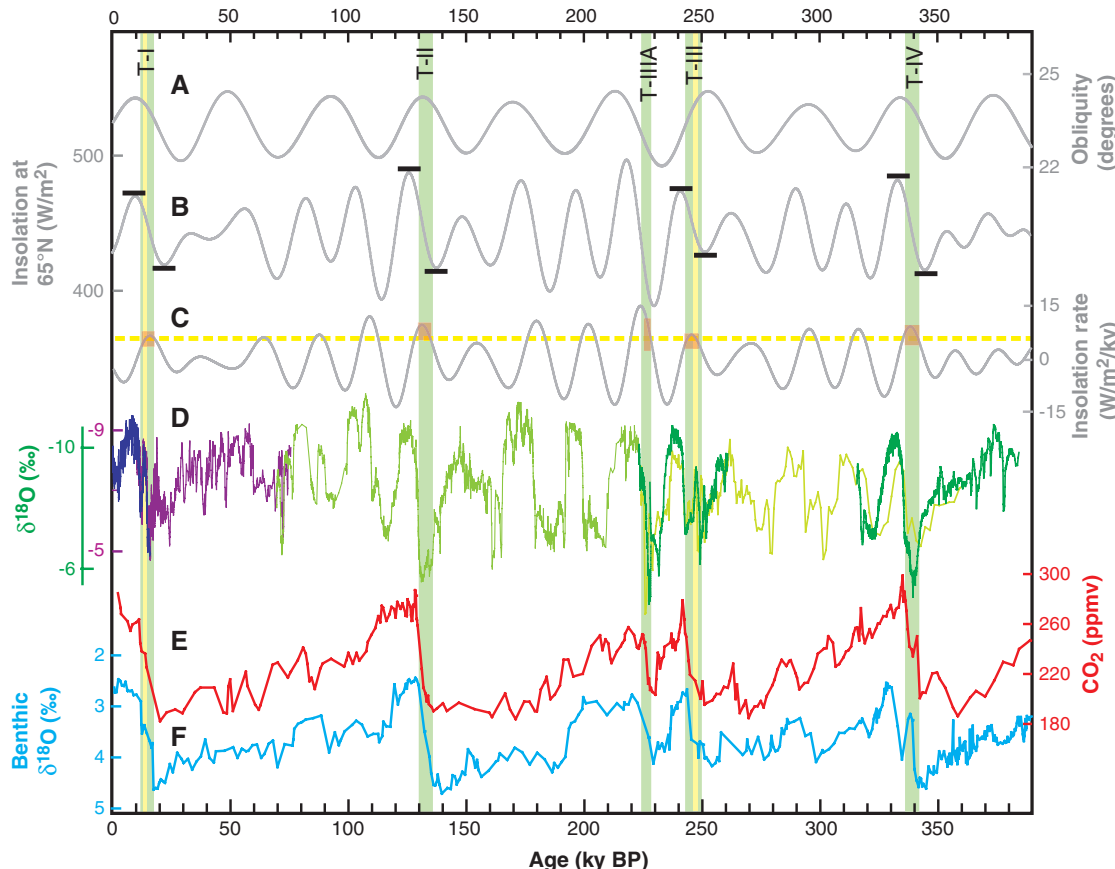
correlating the cave and the Antarctic ice-core records, we observe relationships similar to those of the main terminations for CO_2 and Antarctic temperature. We view this set of events as an extra termination (T-IIIa) that takes place one precession cycle after T-III, which is probably the result of unusually low insolation that rapidly generates a large ice sheet, followed by unusually high insolation that triggers collapse.

Correlations with Antarctic ice cores. As with T-I and T-II (6), abrupt monsoon changes during T-III and T-IV were probably contemporaneous with methane shifts observed in Antarctic cores. We applied this correlation (Fig. 3) to the Vostok (36), Fuji Dome (37), and European Project for Ice Coring in Antarctica (EPICA)/Dome C (38, 39) cores. Ages based on this correlation of the cave chronologies agree within the uncertainties with ages for those cores with O_2/N_2 chronologies [Vostok (40) and Fuji Dome (37)]. We can now add CO_2 , Antarctic temperature/hydrogen isotope ratio (δD), Antarctic dust, and $\delta^{18}\text{O}$ of O_2 to the marine and cave records, all on the cave chronology. For each termination, Antarctic temperature rise takes place during the WMI (or WMIs), broadly paralleling the benthic marine termination and the rising limb of the insolation curve. As in T-I, the rise in temperature during T-III reverses at about the same time as BA-III, a feature we term ACR-III.

For each termination, the CO_2 rise also broadly parallels the marine termination and the in-

solation rise. The idea of a CO_2 rise synchronous with the marine termination differs from some earlier work, which suggested that the marine termination lagged the CO_2 rise by several millennia (41) on the basis of an observed lag in $\delta^{18}\text{O}$ of atmospheric O_2 relative to CO_2 (Fig. 3). The basis for the earlier argument is the known link between $\delta^{18}\text{O}$ of O_2 and $\delta^{18}\text{O}$ of seawater. It is now known that there is also a strong correlation between the $\delta^{18}\text{O}$ of O_2 and Chinese cave $\delta^{18}\text{O}$ (11, 42). This link is reinforced by the observed similarity between $\delta^{18}\text{O}$ of O_2 and Sanbao cave $\delta^{18}\text{O}$ for T-II through T-IV (Fig. 3). On the basis of these relationships, we argue that the main shift in $\delta^{18}\text{O}$ of O_2 during each of the last four terminations results from the abrupt change in the hydrologic cycle, which we observe as the abrupt shift in cave $\delta^{18}\text{O}$ that marks the end of the last WMI in each termination. Because of the ~1 ky residence time of O_2 in the atmosphere (43), the change in $\delta^{18}\text{O}$ of O_2 is more gradual than the cave $\delta^{18}\text{O}$ shift and appears slightly lagged. Ironically, in this view, the change in the $\delta^{18}\text{O}$ of O_2 is related to the termination but, rather than tracking the termination directly, is delayed by the termination itself until the end of the last WMI. The observation that termination and CO_2 rise are broadly synchronous is important because CO_2 can be considered one of the drivers of the termination (along with boreal summer insolation rise). Mechanisms involving positive feedbacks between sea-level and atmospheric CO_2 should now be reconsidered.

Fig. 4. (A) Obliquity (29) and **(B)** 21 July insolation at 65°N (29). Black bars highlight the highest and lowest insolation value bounding each major termination. **(C)** Rate of change of 21 July insolation at 65°N (29). Red shading indicates the timing of the WMIs. The yellow dashed line indicates the lowest maximum for the four terminations. **(D)** $\delta^{18}\text{O}$ from Hulu (purple) (7), Dongge Caves (dark blue) (10), Sanbao Cave [light green (11), dark green (this study)], and Linzhu Cave [yellow-green (this study)]. **(E)** Vostok CO_2 record (36) on a time scale created by interpolating linearly between methane-cave correlation points on each of the four terminations and T-IIIa. **(F)** Benthic $\delta^{18}\text{O}$ values for ODP 980 (8) on a time scale created by interpolating linearly between IRD-cave correlation points on each of the four terminations and T-IIIa. Light green and yellow vertical bars are the same as in Fig. 2.



Termination mechanisms. On the basis of our data, we envision that rising insolation triggers the initial disintegration of a massive, isostatically compensated ice sheet, which in turn triggers a slowing of MOC and hence a lowering of surface-ocean heat flux to the North Atlantic. Along with sea-ice formation, this collapse generates a cold anomaly in the North Atlantic, which weakens the AM through atmospheric teleconnections (26, 27) and also moves the Intertropical Convergence Zone (ITCZ) to the south (44–46). Antarctic temperature increase could result from CO₂ rise, from the bipolar seesaw mechanism (20, 47–51), and from southward shifts in atmospheric circulation patterns (52).

A number of mechanistic ties between this set of events and CO₂ rise seem plausible. First, simple southward movement of climatic zones [observed for ITCZ (45) and southern Brazil (52)] could include a southward shift in the westerlies (53), resulting in enhanced wind-driven upwelling in the ocean around Antarctica, promoting ventilation of respired CO₂, atmospheric CO₂ rise, and observed productivity peaks (54). Second, warming from the bipolar seesaw mechanism could melt sea ice in the Southern Ocean, also promoting CO₂ ventilation (55). Third, warming associated with southerly shifts in climate zones could reduce Patagonian glaciation, lowering the flux of dust and iron from Patagonia to the Southern Ocean, reducing the efficiency of the biological pump (56). There are limits (imposed by bounds on the glacial-interglacial change in the carbonate compensation depth) on the extent to which alkalinity-based mechanisms can contribute to the CO₂ rise (57, 58). However, within these limits, it is plausible that alkalinity-based mechanisms may contribute. Given the broad synchrony between terminations and CO₂ rise, alkalinity-based feedbacks between sea level and atmospheric CO₂, such as the coral reef hypothesis (59), may well contribute once the sea level begins to rise. Archer *et al.* (57) argued that no single mechanism could explain the full glacial-interglacial range in CO₂. Here, we present a scenario in which CO₂ rise could be caused by a set of mechanisms all ultimately linked to the rise in boreal summer insolation. Both rising insolation and rising CO₂ (60–62), generated with multiple positive feedbacks, drove the termination.

References and Notes

- C. Emiliani, *J. Geol.* **63**, 538 (1955).
- W. S. Broecker, J. van Donk, *Rev. Geophys. Space Phys.* **8**, 169 (1970).
- J. D. Hays, J. Imbrie, N. J. Shackleton, *Science* **194**, 1121 (1976).
- Materials and methods are available as supporting material on *Science Online*.
- H. Heinrich, *Quat. Res.* **29**, 142 (1988).
- H. Cheng *et al.*, *Geology* **34**, 217 (2006).
- Y. J. Wang *et al.*, *Science* **294**, 2345 (2001).
- J. F. McManus, D. W. Oppo, J. L. Cullen, *Science* **283**, 971 (1999).
- M. J. Kelly *et al.*, *Palaeogeogr. Palaeoclimatol. Palaeoecol.* **236**, 20 (2006).
- C. A. Dykoski *et al.*, *Earth Planet. Sci. Lett.* **233**, 71 (2005).
- Y. J. Wang *et al.*, *Nature* **451**, 1090 (2008).
- C. H. Hendy, *Geochim. Cosmochim. Acta* **35**, 801 (1971).
- W. Dansgaard, *Tellus* **16**, 436 (1964).
- K. R. Johnson, B. L. Ingram, *Earth Planet. Sci. Lett.* **220**, 365 (2004).
- D. Fleitmann *et al.*, *Quat. Sci. Rev.* **26**, 170 (2007).
- A. Sinha *et al.*, *Geology* **33**, 813 (2005).
- C. Hu *et al.*, *Earth Planet. Sci. Lett.* **266**, 221 (2008).
- R. B. Alley *et al.*, *Nature* **362**, 527 (1993).
- G. Bond *et al.*, *Nature* **365**, 143 (1993).
- W. S. Broecker, D. M. Petet, D. Rind, *Nature* **315**, 21 (1985).
- J. F. McManus, R. Francois, J. M. Gherardi, L. D. Keigwin, S. Brown-Leger, *Nature* **428**, 834 (2004).
- J. C. H. Chiang, M. Biasutti, D. S. Battisti, *Paleoceanography* **18**, 1094 10.1029/2003PA000916 (2003).
- G. H. Denton, R. B. Alley, G. C. Comer, W. S. Broecker, *Quat. Sci. Rev.* **24**, 1159 (2005).
- W. S. Broecker, *Global Planet. Change* **54**, 211 (2006).
- H. F. Blanford, *Proc. R. Soc. London* **37**, 3 (1884).
- T. P. Barnett, L. Dümenil, U. Schlese, E. Roeckner, *Science* **239**, 504 (1988).
- R. Zhang, T. L. Delworth, *J. Clim.* **18**, 1853 (2005).
- G. H. Denton, W. S. Broecker, R. B. Alley, *Pages News* **14**, 14 (2006).
- A. L. Berger, *Quat. Res.* **9**, 139 (1978).
- J. Imbrie *et al.*, in *Milankovitch and Climate, Part I*, A. Berger, J. Imbrie, J. Hays, G. Kukla, B. Saltzman, Eds. (Reidel, Norwell, MA, 1984), pp. 269–305.
- L. G. Thompson *et al.*, *Science* **298**, 589 (2002).
- R. B. Alley, P. U. Clark, P. Huybrechts, I. Joughin, *Science* **310**, 456 (2005).
- G. E. Birchfield, W. S. Broecker, *Paleoceanography* **5**, 835 (1990).
- W. R. Peltier, *Science* **265**, 195 (1994).
- M. E. Raymo, *Paleoceanography* **12**, 577 (1997).
- J. R. Petit *et al.*, *Nature* **399**, 429 (1999).
- K. Kawamura *et al.*, *Nature* **448**, 912 (2007).
- L. Louergue *et al.*, *Nature* **453**, 383 (2008).
- J. Jouzel *et al.*, *Science* **317**, 793 (2007).
- M. Suwa, M. Bender, *Quat. Sci. Rev.* **27**, 1093 (2008).
- N. J. Shackleton, *Science* **289**, 1897 (2000).
- J. P. Severinghaus *et al.*, *Science* **324**, 1431 (2009).
- M. Bender, T. Sowers, L. Labeyrie, *Global Biogeochem. Cycles* **8**, 363 (1994).
- L. C. Peterson, G. H. Haug, K. A. Hughen, U. Röhl, *Science* **290**, 1947 (2000).
- X. F. Wang *et al.*, *Nature* **432**, 740 (2004).
- J. C. H. Chiang, C. M. Bitz, *Clim. Dyn.* **25**, 477 (2005).
- T. J. Crowley, *Paleoceanography* **7**, 489 (1992).
- T. F. Stocker, D. G. Wright, L. A. Mysak, *J. Clim.* **5**, 773 (1992).
- W. S. Broecker, *Paleoceanography* **13**, 119 (1998).
- T. Blunier, E.J. Brook, *Science* **291**, 109 (2001).
- T. F. Stocker, S. J. Johnsen, *Paleoceanography* **18**, 1087 (2003).
- X. F. Wang *et al.*, *Geophys. Res. Lett.* **34**, L23701 10.1029/2007GL031149 (2007).
- J. R. Toggweiler, J. L. Russell, S. R. Carlson, *Paleoceanography* **21**, 2005 (2006).
- R. F. Anderson *et al.*, *Science* **323**, 1443 (2009).
- R. F. Keeling, B. B. Stephens, *Paleoceanography* **16**, 112 (2001).
- J. H. Martin, S. E. Fitzwater, *Nature* **331**, 341 (1988).
- D. Archer, A. Winguth, D. Lea, N. Mahowald, *Rev. Geophys.* **38**, 159 (2000).
- D. M. Sigman, E. A. Boyle, *Nature* **407**, 859 (2000).
- B. N. Opdyke, J. C. G. Walker, *Geology* **20**, 733 (1992).
- D. Paillard, *Rev. Geophys.* **39**, 325 (2001).
- J. P. Severinghaus, *Nature* **457**, 1093 (2009).
- P. U. Clark, A. M. McCabe, A. C. Mix, A. J. Weaver, *Science* **304**, 1141 (2004).
- We thank the late Gary Comer for his generous support and J. Severinghaus, V. Masson-Delmotte, and P. Clark for valuable suggestions. This work was supported by U.S. NSF grant 0502535, Gary Comer Science and Education Foundation grant CC8, NOAA grants to G.H.D., and National Natural Science Foundation of China grants 40631003 and 40771009.

Supporting Online Material

www.sciencemag.org/cgi/content/full/326/5950/248/DC1

Materials and Methods

SOM Text

Figs. S1 to S5

Tables S1 and S2

References

17 June 2009; accepted 14 September 2009

10.1126/science.1177840

Reactome Array: Forging a Link Between Metabolome and Genome

Ana Beloqui,^{1*} María-Eugenio Guazzaroni,^{1*} Florencio Pazos,² José M. Vieites,¹ Marta Godoy,² Olga V. Golyshina,³ Tatyana N. Chernikova,³ Agnes Waliczek,³ Rafael Silva-Rocha,² Yamal Al-ramahi,¹ Violetta La Cono,⁴ Carmen Mendez,⁵ José A. Salas,⁵ Roberto Solano,² Michail M. Yakimov,⁴ Kenneth N. Timmis,^{3,6} Peter N. Golyshin,^{3,7,8†‡} Manuel Ferrer^{1†‡}

We describe a sensitive metabolite array for genome sequence-independent functional analysis of metabolic phenotypes and networks, the reactomes, of cell populations and communities. The array includes 1676 dye-linked substrate compounds collectively representing central metabolic pathways of all forms of life. Application of cell extracts to the array leads to specific binding of enzymes to cognate substrates, transformation to products, and concomitant activation of the dye signals. Proof of principle was shown by reconstruction of the metabolic maps of model bacteria. Utility of the array for unsequenced organisms was demonstrated by reconstruction of the global metabolisms of three microbial communities derived from acidic volcanic pool, deep-sea brine lake, and hydrocarbon-polluted seawater. Enzymes of interest are captured on nanoparticles coated with cognate metabolites, sequenced, and their functions unequivocally established.

Functional genomics has greatly accelerated research on the genomic basis of life processes in health and disease and provided a quantum advance in our understanding of such processes, their regulation, and underlying

mechanisms (*1*). Functional assignments and metabolic network reconstructions have generally depended on both the genome sequence of the organism(s) in question and bioinformatic analyses based on homology to known genes and proteins